Available online at www.sciencedirect.com
ScienceDirect
Ceramics International 37 (2011) 257–264
CERAMICS INTERNATIONAL
www.elsevier.com/locate/ceramint

Influence of sintering parameters on tribological properties of ceria stabilized zirconia bio-ceramics

Ajoy Kumar Pandey, Koushik Biswas *

Department of Metallurgical and Materials Engineering, Indian Institute of Technology, Kharagpur 721 302, India

Received 28 August 2009; received in revised form 23 July 2010; accepted 26 August 2010
Available online 29 September 2010

Abstract

Nano-structured ceria stabilized zirconia powder was synthesized from their respective nitrate salts using a wet chemical co-precipitation method. Dried powder was calcined at different temperatures. Particle size of calcined powders was measured by X-ray diffraction (Scherrer equation) and high resolution transmission electron microscopy. Relative quantities of phases (e.g. monoclinic, tetragonal and cubic) were estimated using rigorous Rietveld analysis. The powder was compacted and sintered conventionally following different time and temperature schedules in order to optimize the sintering schedule for fabrication of dense material. The microstructures of the sintered samples were observed by field emission scanning electron microscopy. Vickers hardness (∼945 VHN) showed appreciable increase (>35%) in the hardness value compared to earlier reported ones. Fretting wear of some of the selected samples was carried out in un-lubricated condition. Wear volume and specific wear rate were estimated and correlated with the microstructure. Fatigue microcrack formation, plastic deformation, grain pull-out and abrasion were found to be the main wear mechanisms.

Keywords: A. Sintering; Ceria stabilized zirconia; Bio-ceramic; Phase analysis; Tribology

1. Introduction

Zirconia, being a bio-inert ceramic, is preferred as a biomaterial for dental and orthopedic (structural) applications since 1969 because of its excellent wear resistance, bio-compatibility and fracture toughness [1,2]. Zirconia ceramics show the best mechanical properties as they undergo transformation toughening that occurs during propagation of a crack inside the matrix. When a crack tries to propagate through a zirconia matrix, the matrix undergoes a diffusionless martensitic type of phase transformation, where the tetragonal phase ($P4_2/nmc$) transforms to monoclinic phase ($P1\ 2_1/c1$) by absorbing some energy from the vicinity of the crack tip [3]. This transformation accompanied by a volume change of about ∼4% results in compressive stress around the crack tip, thereby preventing crack propagation. To exhibit transformation toughening, higher temperature phases (i.e. cubic or tetragonal) need to be stabilized at room temperature. For this purpose, additives like CaO, CeO_2, MgO, Y_2O_3, etc., are normally used as stabilizer.

Among these additives, yttria is the most popular one for stabilization purpose. Although the zirconia–yttria system has good mechanical properties, it shows some long term ageing problem at low temperature regime (200–300 °C) [4]. During 2002–2003, the catastrophic failure events of yttria stabilized zirconia femoral head indicate the problem associated with ageing. Since then, a major challenge is to develop nearly ageing free zirconia bio-ceramic material for these applications [5]. The fracture surfaces of femoral head have been studied by many researchers [6,7] and they found a remarkable increase (up to 30%) of monoclinic phase in the implants during service period. The excessive volumetric strain generated due to phase transformation, if not accommodated, may result in catastrophic failure. This degradation phenomenon is termed as ageing. The key parameters of ageing; like temperature, time, composition and atmosphere dependence were well described by Yoshimura et al. [8].

During ageing, the phase transformation starts first in some isolated grains on the surface by a stress corrosion type mechanism and transforms the neighboring grains subsequently by nucleation and growth process [5]. The transformation of one grain leading to volume increase (∼4%) which causes some

* Corresponding author. Tel.: +91 03222 283244; fax: +91 3222 282280.
E-mail address: k_biswas@metal.iitkgp.ernet.in (K. Biswas).

0272-8842/$36.00
doi:10.1016/j.ceramint.2010.08.041

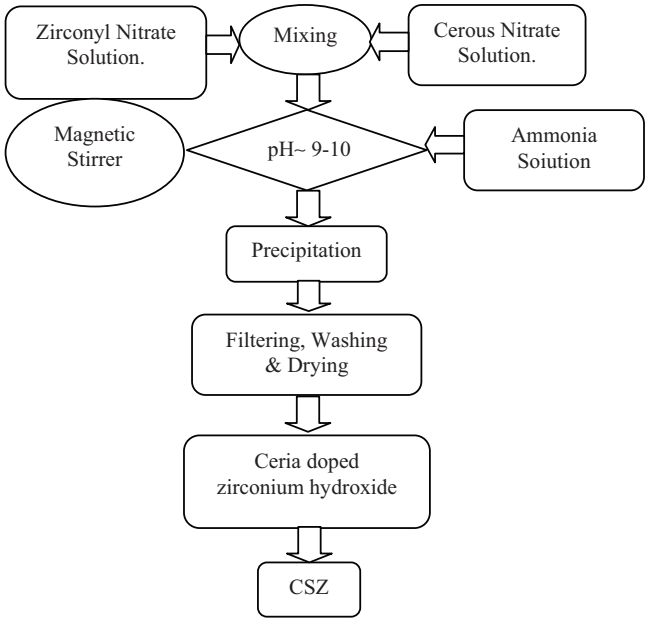

Fig. 1. Schematic representation of the powder preparation process by co-precipitation.

stress to the neighboring grains resulting in interconnected surface and subsurface cracks revealing more and more surface area exposed to the body fluid. This offers an easy channel for body fluid (blood contains about 95% water) to penetrate inside the implants structure [9]. Volume increase due to ageing causes effective surface uplift which roughens the surface and increases the friction between the two surfaces resulting high wear. Wear causes grain pull-out leading to craters at the surface. This eventually leads to the degradation of surface properties or catastrophic failure of the component.

2. Remedy: objective of the study

Ceria stabilized tetragonal zirconia (CSZ) polycrystalline ceramics are attaining greater interest due to their good thermal stability in moist environment, improved mechanical properties and enhanced toughening mechanism [10]. Ceria in zirconia has a wider solid solubility within the tetragonal (zirconia) region [11]. Moreover, it contains an extra advantage over yttria or any other aliovalent (e.g. CaO, MgO, etc.) toughening agent in zirconia ceramics. Use of aliovalent dopants in the zirconia structure creates anionic (oxygen) vacancies (defects) whereas ceria having iso-molecular structure to that of zirconia, does not create any vacancies upon substitution. This can be expressed following the Kröger–Vink notation:

$$Y_2O_3 \xrightarrow{2ZrO_2} 2Y'_{Zr} + V_o^{\bullet\bullet} + 3O_o^{\times} \quad (1)$$

$$CeO_2 \xrightarrow{ZrO_2} Ce_{Zr}^{\times} + 2O_o^{\times} \quad (2)$$

These anionic defects can act as nucleation sites for the formation of the monoclinic phase during ageing. Yttria (or any other aliovalent oxides) stabilized zirconia is expected to have lower anti-ageing properties than the ceria stabilized one. However, due to lack of defects (anionic vacancies) in the structure, CSZ has poor sinterability, as these defects enhance the solid state diffusivities during sintering. In order to overcome the problem of sinterability, a two step (high sintering temperature for shorter holding time followed by low temperature prolonged sintering) sintering schedule is done where defects generated at elevated temperature can be used to densify CSZ by holding at lower temperature. Considering the above mentioned criteria, ceria stabilized zirconia was investigated extensively in terms of optimization of the composition (for complete stabilization) along with calcinations and sintering schedule, tribological and other mechanical properties.

3. Materials and methods

3.1. Processing

8–16 mol% ceria doped zirconia powders were prepared by the co-precipitation method from their respective nitrate salts (cerous nitrate (purity >99.9%), Strem Chemical, USA; and zirconyl nitrate (purity >99.5%), Loba Chemie, India). The precursor salts were dissolved in distilled water in proper ratio and then co-precipitated by dropwise addition of ammoniacal solution as represented in the flow chart (Fig. 1). A pH level of 9–10 was maintained for complete precipitation to occur. The precipitate was then washed, filtered and dried for 12 h at 110 °C. The dried powder was divided into two parts; one part was calcined directly in powder form where the other part was compacted and calcined at

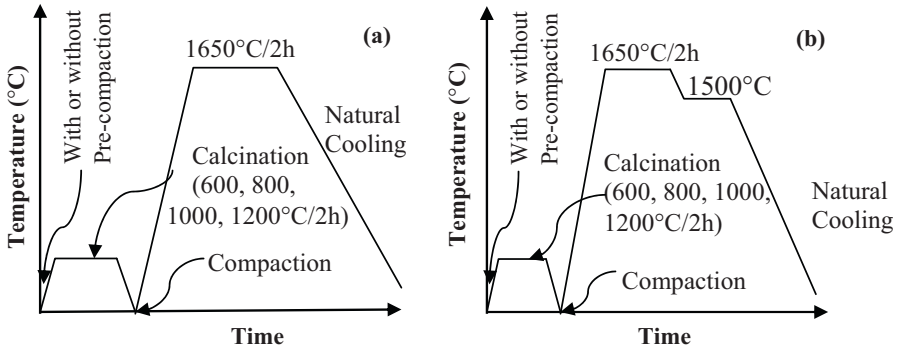

Fig. 2. Different time–temperature schedules followed during sintering: (a) single step and (b) two step.

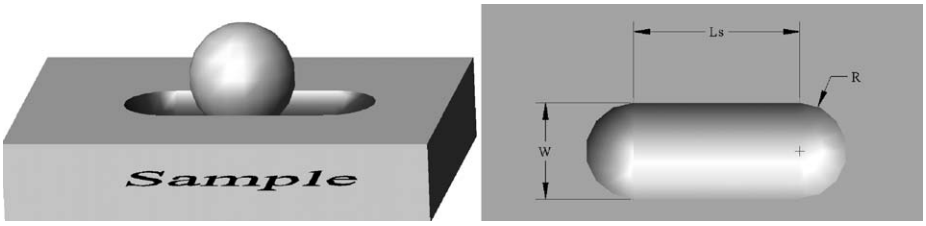

Fig. 3. Schematic representation of wear scar on the ball-on-flat configuration.

different temperatures (600, 800, 1000 and 1200 °C) for 2 h. During calcinations, the synthesized amorphous hydroxide becomes crystalline. The reaction kinetics can be represented as:

$$ZrO(NO_3)_2{\cdot}H_2O + 2NH_4OH \rightarrow Zr(OH)_4 + 2NH_4NO_3 \quad (3)$$

$$2Zr(OH)_4 \rightarrow ZrO_2\,(t) + ZrO_2\,(m) + 4H_2O \quad (4)$$

The calcined powders (if pre-compacted, were crushed into powder) were compacted to 10 mm diameter and 3 mm thick pellets at 600 MPa. Approximately 1 wt% PVA was used as a binder during compaction. The pellets were then sintered following different time–temperature schedules as shown in Fig. 2. Density of the sintered compact was measured by the Archimedes' principle.

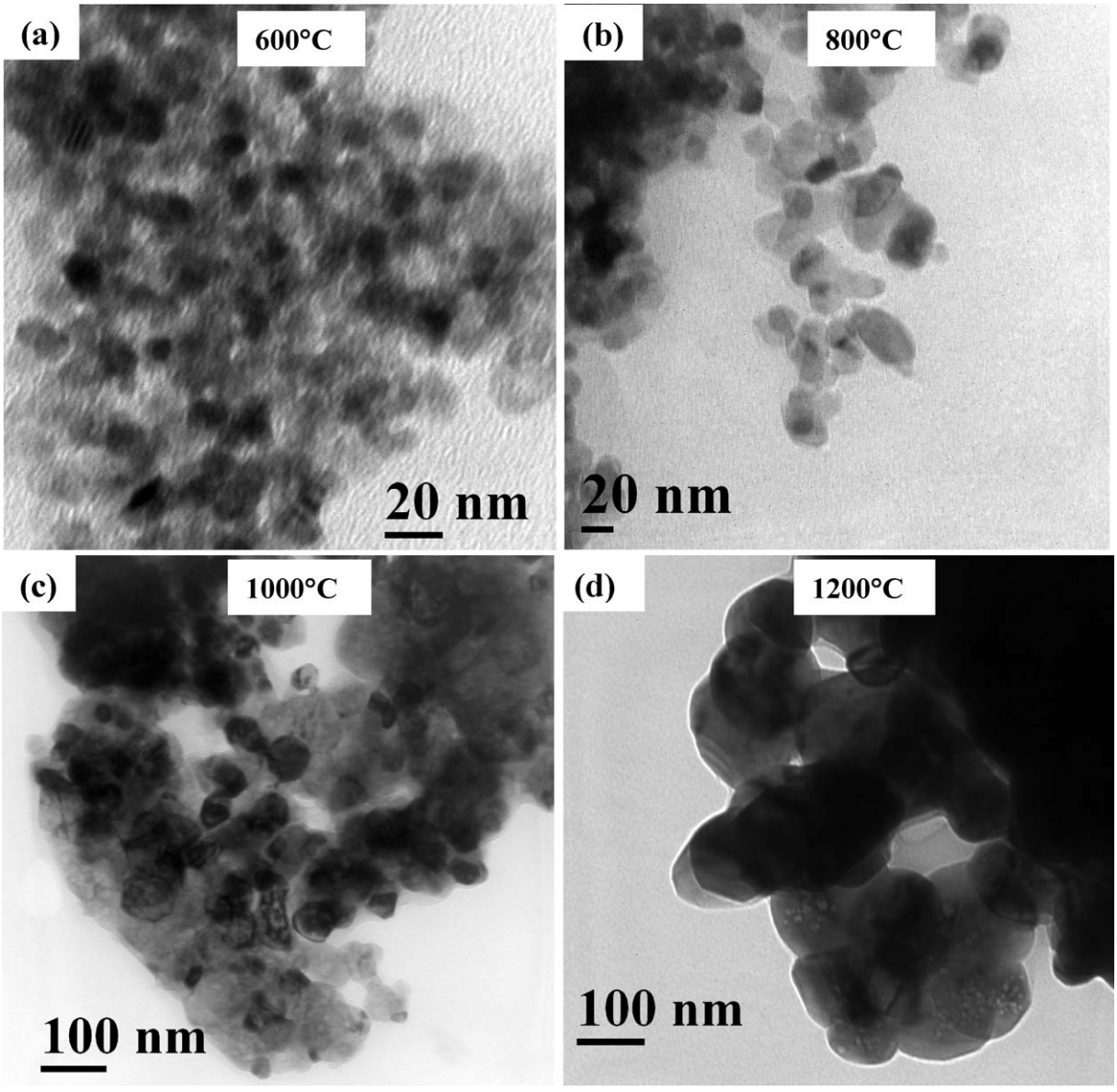

Fig. 4. HRTEM images of 14 mol% ceria doped zirconia powders calcined at (a) 600 °C; (b) 800 °C; (c) 1000 °C and (d) 1200 °C for 2 h.

Table 1
Particle size data and relative phase content in 14 mol% CSZ powder calcined at different temperatures. Rietveld parameters, R_p (profile R factor), R_{wp} (weighted profile), R_{exp} (expected profile) and GOF (goodness of fit) were also provided.

Calcination temperature (°C)	Particle size (nm)		% Phase content		Refinement parameters			
	HRTEM	XRD	Monoclinic	Tetragonal	R_p	R_{exp}	R_{wp}	GOF
600	8	7	1	99	18.95	24.42	24.43	1.001
800	13	13	6	94	18.92	24.56	24.45	1.000
1000	25	26	10	90	20.31	23.89	25.61	1.149
1200	90	45	24	76	20.66	23.08	25.91	1.267

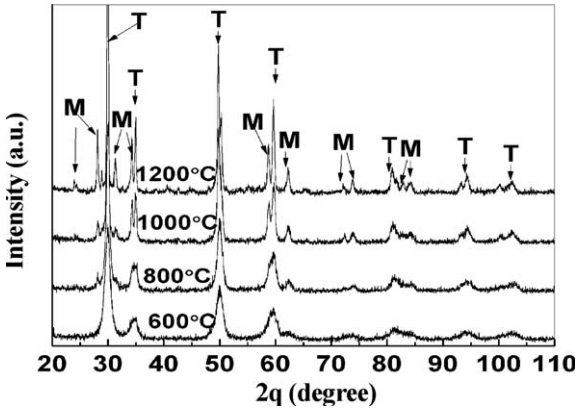

Fig. 5. XRD patterns of 14 mol% ceria doped zirconia calcined at different temperatures as indicated (T: tetragonal and M: monoclinic phase).

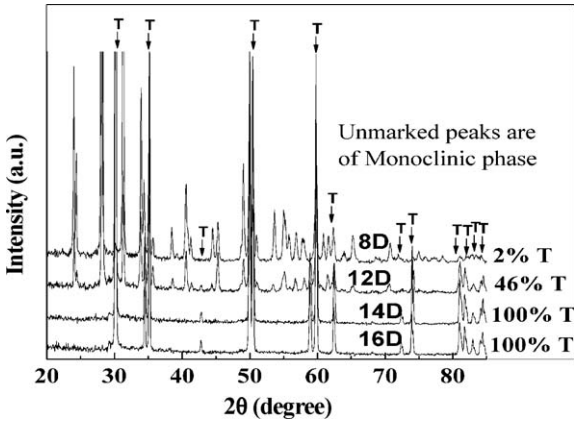

Fig. 6. XRD patterns of different CSZ samples sintered at 1700 °C for 2 h in air. The patterns show that at least 14 mol% ceria is required for total stabilization of tetragonal phase. (Numeric value stands for mol% stabilizer (D).)

3.2. Microstructure, phase analysis and mechanical properties

Sintered pellets were diamond polished and thermally etched at 1200 °C for 1 h and observed by scanning electron microscopy (SEM) (SUPRA-40, Carl Zeiss, Germany). Powders and sintered specimens were characterized by XRD (PANalytical, X'Pert PRO, Phillips) for crystallite sizes and quantitative phase analyses. Particle sizes of different calcined powders were estimated by transmission electron microscopy (TEM) (JEM 2100, Geol, Japan). The relative amount of the phases was calculated by a rigorous Rietveld analysis of the XRD patterns using the software, X'Pert Highscore Plus (PANalytical B.V.,

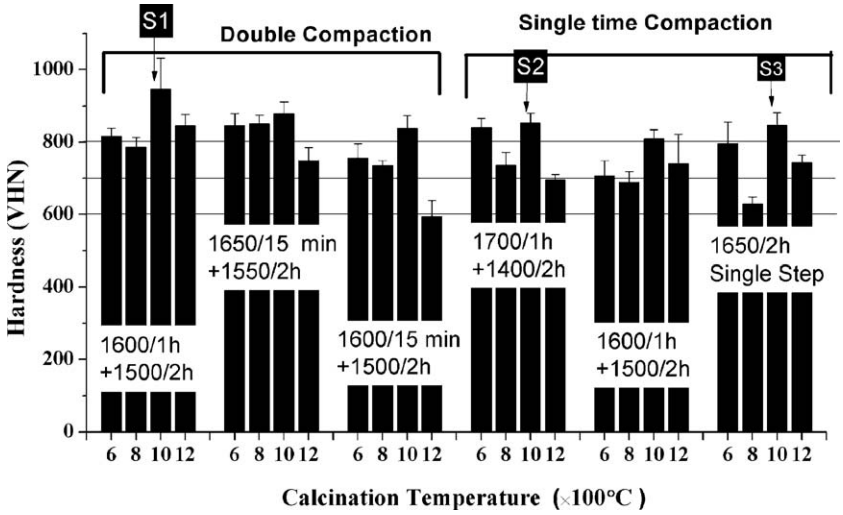

Fig. 7. Effect of calcination and sintering schedules on hardness of 14 mol% CSZ. X-axis values [(6, 8, 10, 12) × 100 °C] denote calcination temperatures. The sintering schedules (temperature in °C/time) are presented in each column.

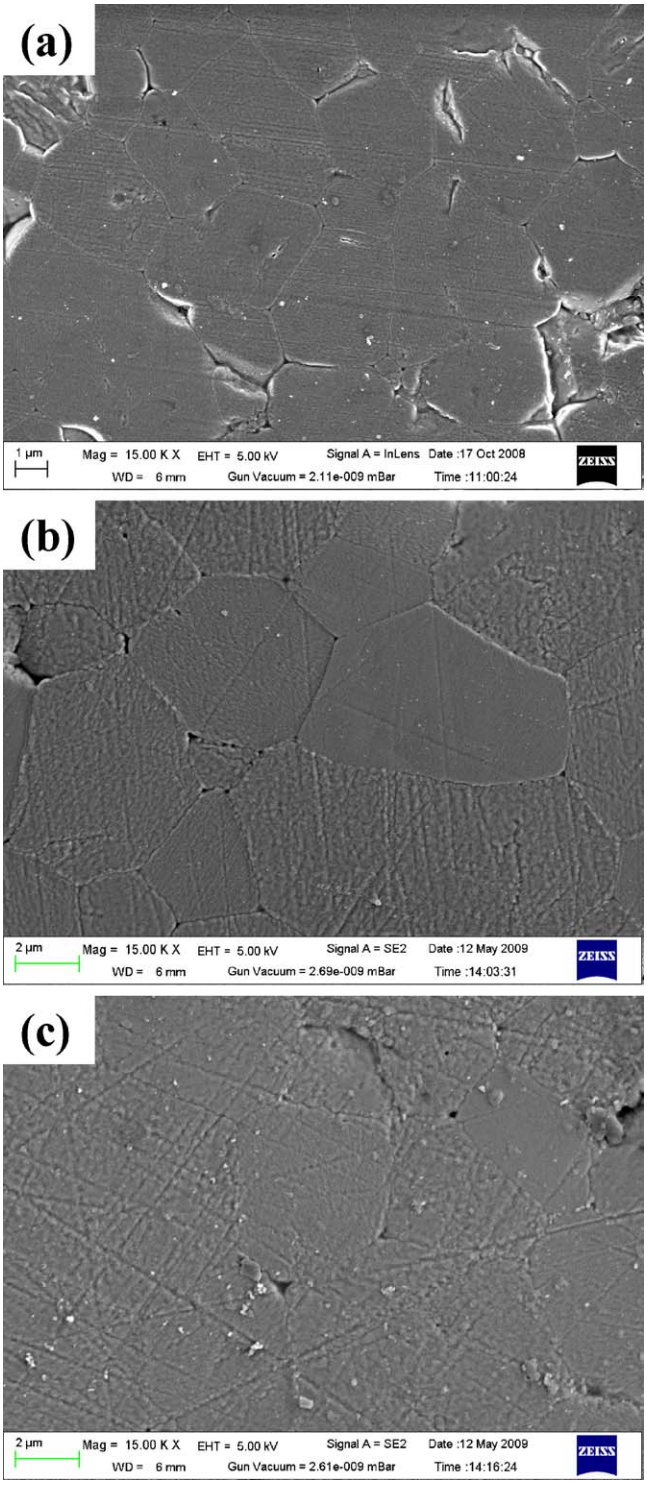

Fig. 8. SEM images of polished and thermally etched specimens of (a) S1; (b) S2; and (c) S3 showing the faceted grain morphology. Small polishing pull-outs can be observed on the surface.

Almelo, The Netherlands). To eliminate the instrumental broadening, standard coarse grained samples were prepared using similar compositions.

Vickers indentation hardness was measured in bulk sintered specimens following the standard procedure using 200 N load [12].

3.3. Tribology

Un-lubricated fretting wear for 10^5 cycles was carried out using a fretting wear tester (TR-283M-M4, Ducom, India) taking yttria stabilized zirconia (YSZ) ball as counter body (ball-on-flat configuration). The surface roughness of specimens and the counter body were measured using a surface profilometer (Veeco Dektak 150 Surface Profilometer, USA). The average rounding radius, R_a and R_t surface roughness of the ball were determined to be 10.00 mm, 0.023 μm and 0.07 μm, respectively. The R_a and R_t surface roughness of specimens were found to be 0.2–0.35 μm and ~1.0 μm, respectively. The contact load was varied from 30 N to 50 N, with a stroke length of the oscillating motion and frequency of 1 mm and 10 Hz, respectively. Wear volumes were estimated neglecting the geometric errors due to directional reversal at the ends and considering zero wear of the sliding ball. A schematic drawing of the wear scar is shown in Fig. 3. The wear scar consists of two spherical portions at the two ends and a cylindrical portion at the centre. According to this geometry, the wear volume (V_w) can be calculated as:

$$V_w(L,R,h) = L_S\left[R^2\ \cos^{-1}\left(\frac{R-h}{R}\right) - (R-h)\sqrt{2Rh-h^2}\right] + \frac{1}{3}\pi h^2(3R-h) \tag{5}$$

where L_s is stroke length, R is radius of the sliding ball and h is the wear depth.

The specific wear rate (in $mm^3/N\,m$) was calculated according to the following formula [13]:

$$k_w = \frac{V_w}{FS}\ (mm^3/N\,m) \tag{6}$$

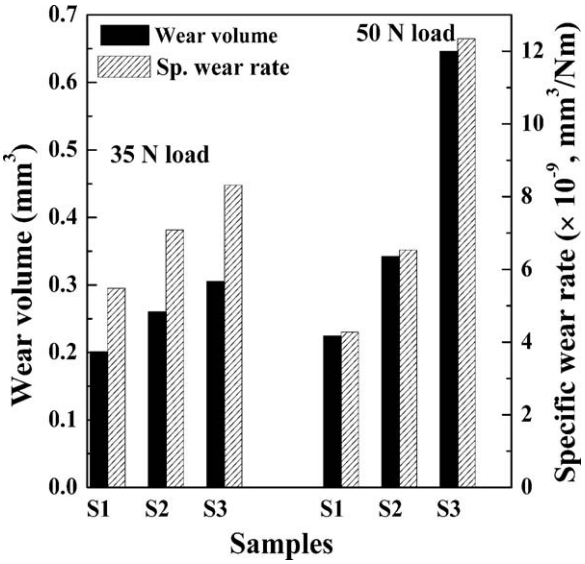

Fig. 9. Specific wear rates and wear volumes of the samples S1, S2, and S3 fretted under 35 N and 50 N load.

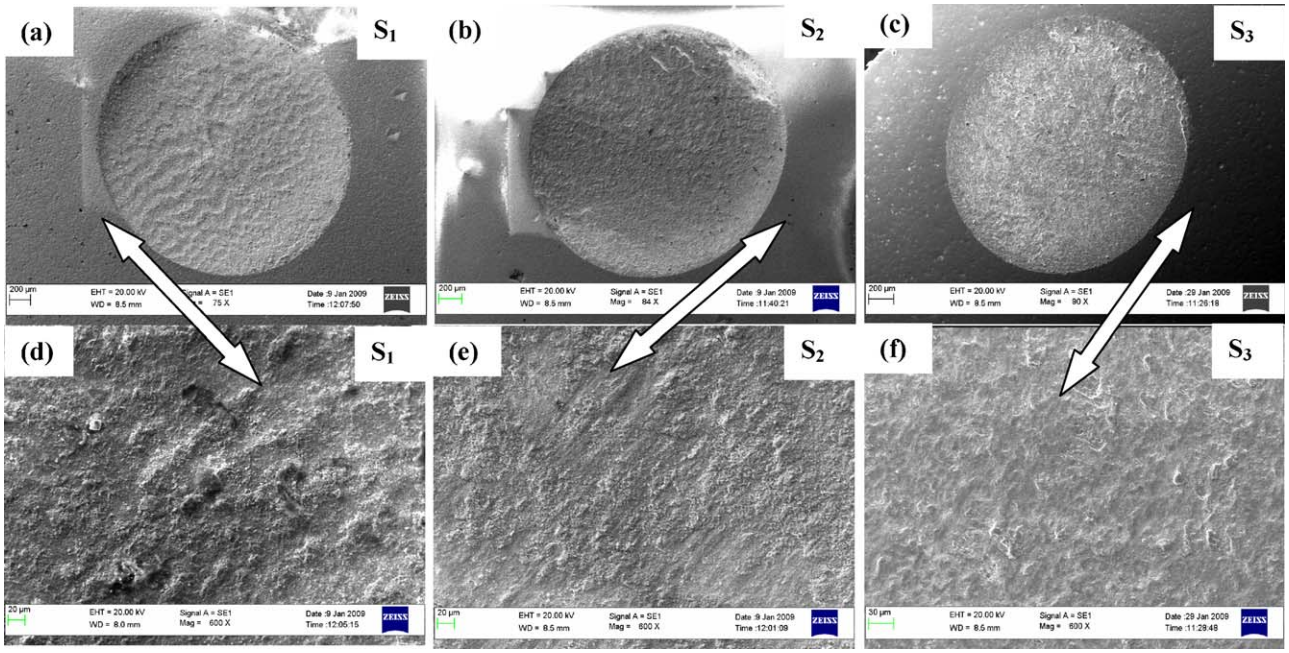

Fig. 10. FESEM images show wear scars (a)–(c) and worn surfaces (d)–(f) after fretting test at 35 N load. Double arrows show the direction of oscillatory motion.

where V_w is the wear volume (mm^3), F is the applied force (N), S is the sliding distance (m). The worn surfaces were also observed by SEM and qualitative elemental analyses were done on the worn surfaces and of the wear debris by EDX analysis.

4. Results and discussions

4.1. Optimization: composition and sintering schedule

Transmission electron microscopy (TEM) images of different CSZ nano-particles, Fig. 4, show that the particles are crystalline and have uniform size distributions. The mean particle size increases with the increase in calcination temperatures (Table 1). Fig. 5 shows the XRD patterns obtained from the calcined powders. The average crystallite sizes and relative phase contents were refined by Rietveld analysis (Table 1). Except for the 1200 °C calcined one, the average particle sizes observed by TEM almost match with the particle size calculated by the Scherrer (XRD) formulae. During calcination at higher temperature (1200 °C), bicrystalline particles (containing two crystallites) are formed. Hence the average crystallite size measured by XRD is almost half of the particle size observed by TEM.

Phase analyses reveal that 600 °C calcined powder possesses almost 99% tetragonal phase and with the increase in calcination temperature, the monoclinic (M) to tetragonal (T) phase ratios increase. With the increase in the particle size, the specific surface area decreases, thereby decreasing the total surface energy (total energy of the system as well) which mainly accounts for the stabilization of high temperature phase (T) at room temperature.

Powders containing 8, 10, 12, 14 and 16 mol% ceria were sintered at 1700 °C for 2 h to optimize the minimum ceria content required for total stabilization of tetragonal phase after sintering. The XRD patterns (Fig. 6) of the sintered samples show that a minimum 14 mol% ceria is required for 100% stabilization of the tetragonal phase at room temperature.

Single step, two steps and two steps double pressing sintering of the samples following different time–temperature schedules (Fig. 2) were carried out. Sintered densities greater than 95% were measured for all the specimens. Out of these, samples prepared from 1000 °C calcined powders showed best results in terms of hardness value (Fig. 7). Average sintered densities of these specimens were found to be near the theoretical one. It seems that there is a trade-off between the initial particle size, sintering time and temperature, and final grain size of the sintered material. As hardness is an extrinsic property, i.e., it depends on the final density and the grain size, the highest hardness value obtained from each set (single step, double step with and without double compaction) was taken as guideline for selecting the samples designated as S1, S2 and S3. The SEM micrographs (Fig. 8) of these selected specimens showed a faceted grains structure of average sizes between 2 and 3 μm. It is observed that double pressing and double sintering (sample S1) provides better sintering with relatively finer microstructure and an average hardness value up to 945 VHN20 is obtained which is almost 35% greater than the reported one [14–16].

4.2. Wear and frictional analysis

Fig. 9 shows the tribological parameters calculated after the fretting wear test. Sample S1 shows the lowest specific wear rate and wear volume as compared to the other two specimens. Although having similar composition, the wear rate for the harder material (S1 possesses the highest hardness) was found

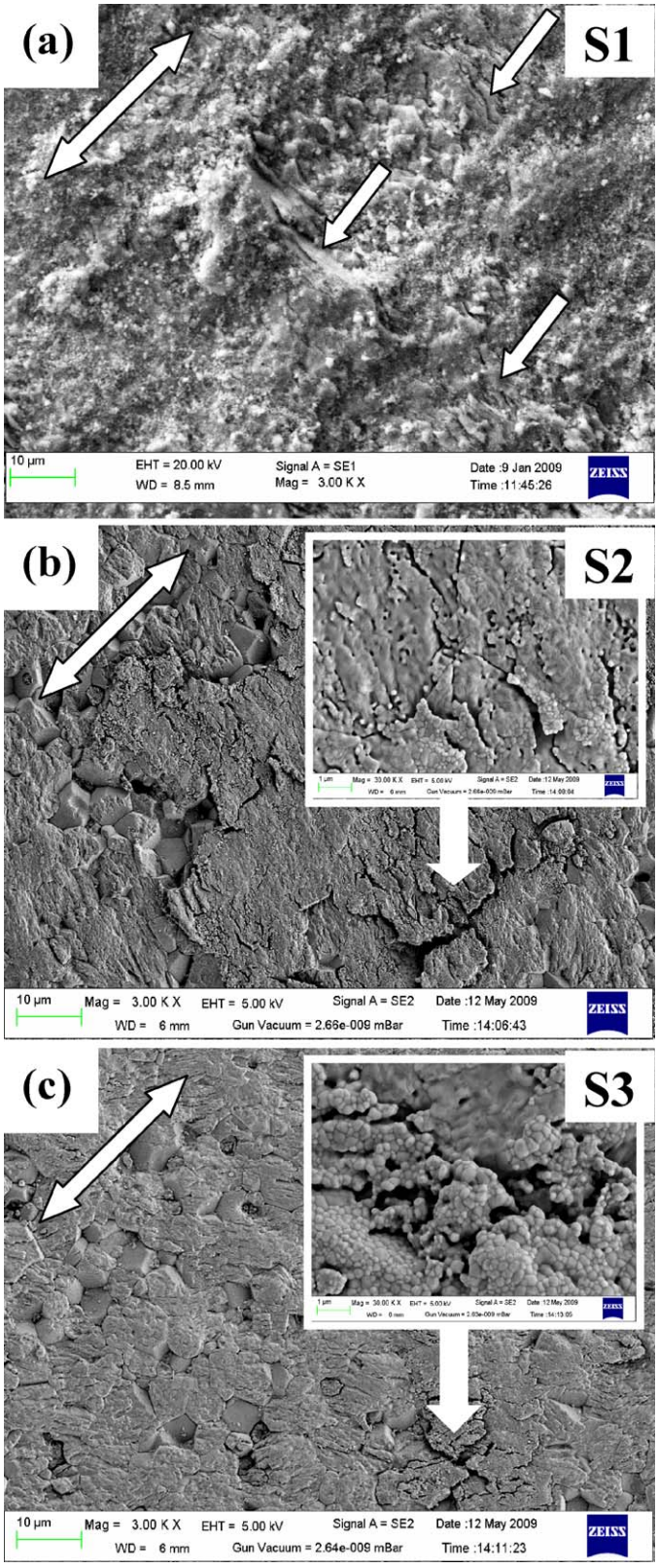

Fig. 11. High magnification worn surfaces showing fatigue microcracks indicate by arrow (in (a)) and plastically deformed adhered layers (in (b) and (c)). Inset micrographs in (b) and (c) show sintering of nano-particles (wear debris) formed due to abrasive wear. Double arrows show the direction of oscillatory motion.

to be minimum. Microstructures of the wear scar and worn surfaces were examined (Fig. 10). It was observed that the wear pit in S1 (Fig. 10(a)) was quite rough as compared to the other two specimens. A close examination of the wear tracks reveals presence of microcracks oriented perpendicular to the fretting direction in S1 (Fig. 11(a)) sample. The observed surface fatigue cracks on the worn surface formed due to transformation of tetragonal to monoclinic zirconia induced by the mechanical stress at the tribocontacts [17]. This toughening causes less wear and debris formation in sample S1. On the contrary, the worn surfaces of S2 and S3 (Fig. 11(b) and (c)) show accumulation of wear debris at the surface. The wear debris got plastically deformed and adhered to the surface of the grains. Jansen et al. [18] also observed similar behavior in ceria doped Y-TZP. The accumulation of wear debris was possible because of the dry test conditions and the horizontal position of the sample. Inset micrographs in Fig. 11(b) and (c) show fine CSZ particles (wear debris) sintered on the wear surfaces of the specimens. The removed grains act as third body resulting in an increase of abrasive wear [18]. One can conclude that the wear mechanisms in these two samples were mainly grain pull-out and abrasion (microcutting and microploughing) leading to higher wear rate as compared to the sample S1.

5. Conclusions

Ceria stabilized zirconia ceramics can be successfully consolidated to near full density by following proper time–temperature sintering schedules. Poor sinterability of CSZ requires a prolong heating at higher temperatures thereby resulting in higher grain growth. The hardness value up to 945 VHN20 with better wear resistive properties can be achieved. Depending on the processing route, one can produce a tougher CSZ with high hardness value. The major wear mechanisms were found to be surface fatigue with microcrack formation, plastic deformation, grain pull-out and abrasion (micro-cutting/ploughing).

References

[1] S. Deville, J. Chevalier, et al., Low-temperature ageing of zirconia-toughened alumina ceramics and its implication in biomedical implants, J. Eur. Ceram. Soc. 23 (2003) 2975–2982.
[2] P.P. Lutton, B. Ben-Nissan, The status of biomaterials for orthopedic and dental applications: part I—materials, Mater. Tech. 12 (1997) 119–126.
[3] E.C. Subbarao, H.S. Maity, K.K. Srivastava, Martensitic transformation in zirconia, Physica Status Solidi (A) 21 (1972) 9–40.
[4] J.-H. Park, S.-W. Moon, Stability and sinterability of tetragonal zirconia polycrystals costabilized by CeO_2 and various oxides, J. Mater. Sci. Lett. 11 (1992) 1046–1048.
[5] J. Chevalier, What future for zirconia as a biomaterial? Biomaterials 27 (2006) 535–543.
[6] K. Haraguchi, N. Sugano, T. Nishii, H. Miki, K. Oka, H. Yoshikawa, Phase transformation of a zirconia ceramic head after total hip arthroplasty, J. Bone Joint Surg. [Br.] 83-B (2001) 996–1000.
[7] P. Hernigou, T. Bahrami, Zirconia and alumina ceramics in comparison with stainless-steel heads: polyethylene wear after a minimum ten year follow-up, J. Bone Joint Surg. [Br.] 85-B (2003) 504–509.
[8] M. Yoshimura, T. Noma, K. Kawabata, S. Sōmiya, Role of H_2O on the degradation process of Y-TZP, J. Mater. Sci. Lett. 6 (1987) 465–467.

[9] J. Chevalier, B. Cales, J.M. Drouin, Low temperature aging of Y-TZP ceramics, J. Am. Ceram. Soc. 82 (1999) 2150–2154.
[10] R. Matsumoto, Ageing behavior of Ce-stabilized tetragonal zirconia polycrystals, J. Am. Ceram. Soc. 71 (1978) 128–129.
[11] K. Tsukuma, M. Shimada, Strength, fracture toughness and Vickers hardness of CeO_2-stabilized tetragonal ZrO_2 polycrystals (Ce-TZP), J. Mater. Sci. 20 (1985) 1178–1184.
[12] M. Barsoum, Fundamentals of Ceramics, McGraw-Hill, Singapore, 1997.
[13] J. Wang, R. Stevens, Review zirconia-toughened alumina (ZTA) ceramics, J. Mater. Sci. 24 (1989) 3421–3440.
[14] S.C. Sharma, N.M. Gokhle, R. Dayal, R. Lal, Synthesis, microstructure and mechanical properties of ceria stabilized tetragonal zirconia prepared by spray drying technique, Bull. Mater. Sci. 25 (2002) 15–20.
[15] J.-D. Lin, J.-G. Duhb, Fracture toughness and hardness of ceria- and yttria-doped tetragonal zirconia ceramics, Mater. Chem. Phys. 78 (2002) 253–261.
[16] J. Wang, X.H. Zheng, R. Stevens, Fabrication and microstructure–mechanical property relationships in Ce-TZPs, J. Mater. Sci. 27 (1992) 5348–5356.
[17] B. Basu, R.G. Vitchev, J. Vleugels, J.P. Celis, O. van der Biest, Fretting wear of self-mated tetragonal zirconia ceramics in different humidity, Key Eng. Mater. 206–213 (2002) 783–786.
[18] S.R. Jansen, A.J.A. Winnubst, Y.J. He, H. Verweij, P.G.Th. van der Varst, G. de With, Effects of grain size and ceria addition on ageing behaviour and tribological properties of Y-TZP ceramics, J. Eur. Ceram. Soc. 18 (1998) 557–563.